

Optical Emission Spectroscopy of Zinc Oxide Doped Nickel Oxide to Calculate Plasma Parameters Using the Boltzmann Plot Method

Muna A. Issa^{1*} and Kadhim A. Aadim¹

¹*Department of Physics, College of Science, University of Baghdad, Iraq*

*Corresponding author: muna.ahmed@sc.uobaghdad.edu.iq

Kadhim A. Aadim is a journal editor, but he participated only as an author in the peer review process. The authors declare no other conflicts of interest.

Abstract

The study used optical emission spectroscopy to present the effect of changing doping ratios and laser energy on plasma parameters. Plasma spectra were acquired across energy levels by zinc oxide combined with nickel oxide (ZnO_xNiO_{1-x}) at $x = 0.3, 0.5,$ and 0.7 . The analysis of these airborne mixtures was carried out through spectroscopy. The electron temperature results indicated that the range for $x=0.3$ was $0.446-0.491$ eV, for $x=0.5$ was $0.470-0.486$ eV, and for $x=0.7$ it was $0.474-0.489$ eV. Differences in electron temperatures between compositions can lead to new technological applications and comprehension of physical phenomena. It was found that when the proportion of doping was increased, the intensities of the spectral lines, electron temperature (T_e), Debye number (N_D), and Debye length (λ_D) increased. On the other hand, as the laser energy increased, the electron density (n_e) and plasma frequency (f_p) went down. At the same time, the emission lines from the doped material appeared more often in the mixed material. These results provide the best conditions for solar cell applications for zinc oxide elements combined with nickel oxide.

Article Info.

Keywords:

Zinc Oxide (ZnO), Optical Emission Spectroscopy (OES), Boltzmann-Plot, Nickel Oxide (NiO), Laser Ablation.

Article history:

Received: Jun. 16, 2024

Revised: May, 27, 2024

Accepted: Jul. 08, 2024

Published: Jun.01, 2025

1. Introduction

Laser Induced Breakdown Spectroscopy (LIBS) is a contemporary analytical method rooted in emission spectroscopy. It uses an intense energy laser directed onto a sample to induce vaporization and excitation. This process effectively elevates the species within the sample to higher energy states, from which they subsequently emit characteristic radiation upon decay. This emitted radiation is then captured, filtered through a wavelength selector, and ultimately detected. It is worth noting that this technique applies to samples in various states, including solids, liquids, and gases [1]. LIBS has tremendous potential for a wide range of applications. LIBS-based sensors are used in numerous fields, including security and industry [2], geological and mineralogical substances [3], cultural legacy [4], biomedicine (such as bacterial identification), inspection at depth, space exploration (e.g., using LIBS- sensors in Chem Cam and Super Cam affixed to the NASA Mars rovers Curiosity and tenacity to analyze Martian rocks), measurements of the environment [5] and facilitate the straight forward production of multilayered films comprising various materials [6].

It is a well-established phenomenon that laser-induced air disintegration occurs during laser-solid interaction at nanosecond and microsecond irradiation regimes in an open atmosphere [7], which can be induced by a variety of factors, air humidity in particular [8]. Inverse bremsstrahlung takes place as air plasma forms before the conclusion of the laser pulse, enabling free electrons to absorb the incoming laser light efficiently. These electrons acquire adequate energy to surpass the ionization potential, breaking the ionization barrier. They produce secondary electrons upon collision with



neutral gas species' atoms and molecules. Subsequently, these molecules absorb radiation and generate further electrons through the same process. This exponentially developing phenomenon is referred to as an avalanche, and it is the cause of air disintegration. This procedure is illustrated in Fig. 1 [9].

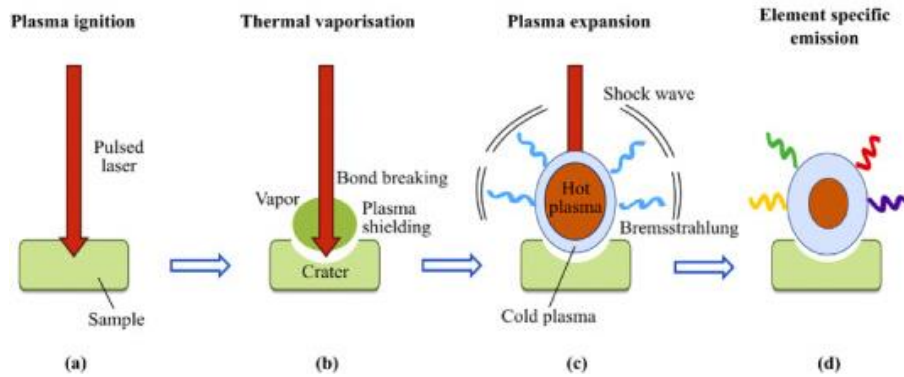


Figure 1: Diagram of induced breakdown by laser [9].

Exposure of certain substances to laser within a liquid can result in the generation of nanoparticles. This process, known as laser ablation or laser-induced breakdown, involves focusing a laser beam onto a target material submerged in a liquid [10]. Plasma diagnostics can be assessed by determining the electron temperature (T_e) and the electron density (n_e). Optical emission spectroscopy (OES) is the diagnostic method used for plasma analysis [11]. It takes a line devoid of self-absorption to determine the electron density using the Stark broadening effect [12]. Self-absorption is a condition that can manifest itself in virtually any system with the ability to emit radiation, including plasma. Furthermore, the process of plasma formation in the air typically exhibits a significant temperature gradient due to the cooling effect of the ambient air [13]. In the outer regions of the cold plasma, elevated atom concentrations exist in lower energy states. Consequently, this situation could result in a noteworthy reabsorption of the emitted radiation lines [14]. A spectrograph and a detector are utilized to detect the plasma plume and achieve spectral resolution. Information regarding the elemental composition and various quantitative and qualitative data can be collected from the generated plasma spectrum. The widths, variations, and shapes in the emission lines offer insights into the temperature and electron density of the plasma.

Plasma temperature holds significant importance as a thermodynamic property, as it characterizes and forecasts other plasma attributes, such as the distribution of energy level populations and particle speeds. Assuming plasma thermodynamic equilibrium. The line intensity ratio method was used to measure the electron temperature of the plasma. Plasma generation that occurs within a few hundred nanoseconds and irradiances above 10^8 W/cm^2 can be easily observed using LIBS. It has been approximated that LTE (Local Thermodynamic Equilibrium) is typically attained in the atmosphere. The line intensity ratio method is a widely used approach for determining plasma temperature. It operates by comparing the intensity ratio of two spectral lines to identify which atom or ion is at the same ionization stage [15]. The plasma temperature (T) in LTE is determined using Eq. (1) [16]

$$T = \frac{(E_2 - E_1)}{k \ln\left(\frac{I_1 \lambda_1 A_2 g_2}{I_2 \lambda_2 A_1 g_1}\right)} \quad (1)$$

where A represents the probability of the occurring transition, I is the intensity, E is the excited state's energy in electron volts, and k is the Boltzmann constant.

Electron density refers to the quantity of free electrons within a given volume. Determining electron density is possible via various reliable methods, such as Thomson scattering, microwave, and plasma spectroscopy. Within this laboratory context, utilizing the linear Stark broadening of spectral lines proves to be a reliable technique for determining electron density. The primary factors contributing to line broadening in LIBS plasmas are the Stark effect and Doppler width. The Doppler width is solely determined by the emitting species atomic mass and temperature. This broadening is not considered significant in this experiment because the hydrogen line's Doppler width employed typically falls within the range of 0.04 to 0.07 nm. Considered a form of pressure broadening, the Stark effect is caused by the interaction between adjacent particles and radiators. These interactions occur in plasmas due to ion collisions and, to a lesser degree, electron collisions. The primary factor contributing to the broadening of the hydrogen line is attributed to the Stark effect [17].

The Saha-Boltzmann equation used consecutive ionization stages and spectral lines of a given element. The Saha-Boltzmann equation is typically expressed as in Eq. (2) [18]

$$n_e = \frac{I_Z^*}{I_{Z+1}^*} 6.04 \times 10^{21} \left(T^{\frac{3}{2}} \right) \times \exp \left[\left(-E_{K,Z+1} + E_{K,Z} - x_Z / K_B T \right) \right] \text{ cm}^{-3} \quad (2)$$

where $I_Z^* = I_Z \lambda_{ki,Z} / g_{K,Z} A_{ki,Z}$, is the modified line intensity for the transition in stage Z, I_{Z+1}^* : Modified line intensity for the transition in stage (Z+1), $E_{K,Z+1}, E_{K,Z}$: Ionization energy for the states (K, Z+1) and (K, Z) respectively, $\lambda_{ki,Z}$: the wavelength of the k-i transitions. $g_{K,Z}$: the statistical weight of the transition, $A_{ki,Z}$: denotes the ionization energy of the species in ionization stage Z, I_Z : the change in wavelength of the transition from level-2 to level-1.

The calculation of the plasma frequency (f_p) is carried out using Eq. (3)

$$f_p \cong 8.98 \sqrt{n_e} \text{ (Hz)} \quad (3)$$

The frequency is a fundamental characteristic of plasma entirely determined by plasma density.

The Debye shielding phenomenon occurs when charged particles weaken the intensity of nearby electric fields. This shielding effect significantly contributes to establishing the quasi-neutrality of the plasma. The Debye length (λ_D) is a characteristic length scale that is defined as in Eq. (4) [19]

$$\lambda_D = \left(\frac{\epsilon_0 k T_e}{n_e e^2} \right) = 43 \sqrt{\frac{T_e}{n_e}} \quad (4)$$

where e represents the electron charge (C), and ϵ_0 denotes vacuum permittivity. The Debye length ought to be exceedingly small compared to the system dimensions; this is the initial requirement for the existence of plasma. $\lambda_D \ll L$ signifies that the Debye length is significantly smaller than the system dimension (L). The second requirement for the existence of plasma is that $N_D \gg 1$, which means in Eq. (5) [20]

$$N_D = \frac{4\pi}{3} n_e \lambda_D^3 \quad (5)$$

This study aims to generate plasma through the pulsed laser technique applied to nickel oxide doped with zinc oxide, investigate its parameters, such as electron density, plasma frequency, electron temperature, Debye number (N_D), and Debye length, and discern the nature of the relationships among these parameters.

2. Experimental Work

The spectrum of the light emitted from the zinc oxide doped nickel oxide ($\text{ZnO}_x\text{NiO}_{(1-x)}$) plasma in air ($x = 0.3, 0.5,$ and 0.7) using the LIBS (laser-induced breakdown spectroscopy) technique was recorded. The setup is shown in Fig. 2.

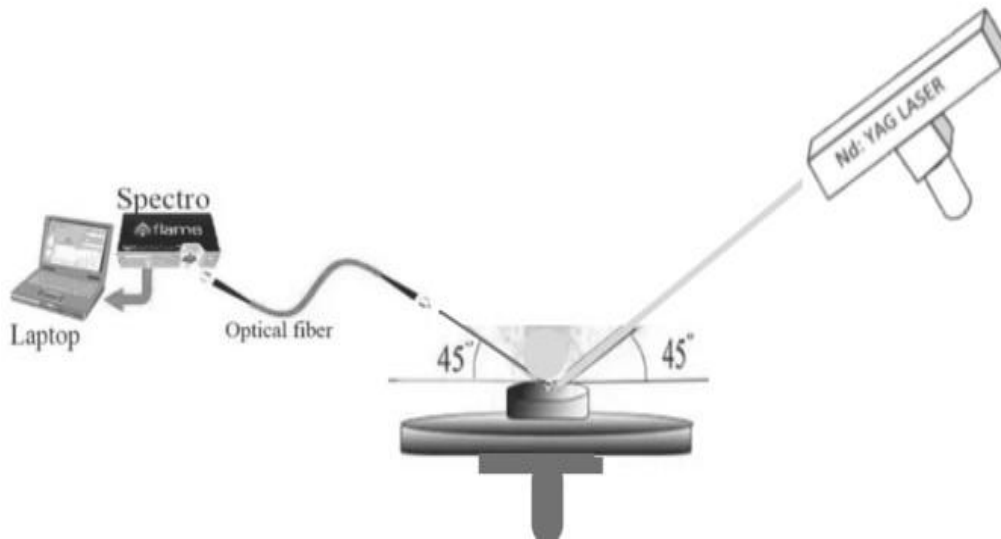


Figure 2: The LIBS system set-up.

It consists of a 1064 nm wavelength pulsed Nd:YAG laser of 9 ns duration, 6 Hz repetition frequency, and 700-1000 mJ energy. The sample's surface, located inside a convergent lens with a focal length of 10 cm, is the focus of the laser beam. The optical fiber makes a 45° angle with the target, and the distance from the plasma sample is 5 cm. The wavelength range that the spectrum analyzer can detect is 200–700 nm. To validate the findings, they were cross-referenced with NIST records. In addition, several plasma parameters were assessed, including electron density and electron temperature.

3. Results and Discussion

Fig. 3(a, b, and c) presents the laser-generated optical emission spectra of ($\text{ZnO}_x\text{NiO}_{1-x}$) plasma with x values of 0.3, 0.5, and 0.7 were recorded in air, covering wavelengths from 200 to 700 nm, using laser energies of 700, 800, 900, and 1000 mJ. The figure illustrates that the intensity of the spectral lines increases with increasing the laser energy. The target's ablation rate increases when the laser energy goes up, the target's ablation rate goes up. This means that more excited atoms are created, which leads to higher spectral intensity. This result was also reported by Ismeal [21] and Abdullah et al. [22].

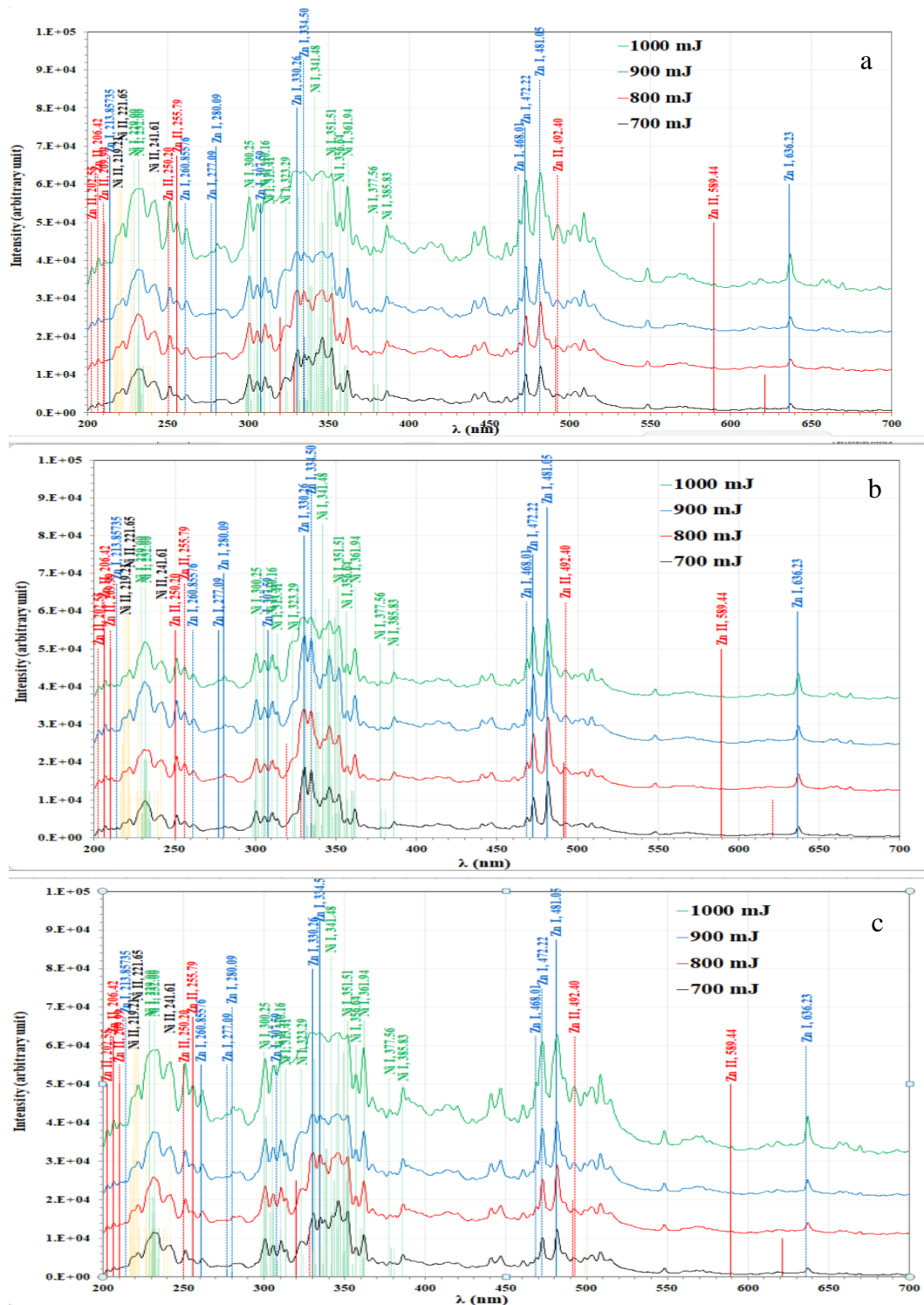


Figure 3: (a) The plasma optical emission spectra for ZnO_xNiO_{1-x} target with $x=0.3$ (b) $x=0.5$ (c) $x=0.7$ under different laser energy.

Tables 1-3 show estimated values for ZnO_xNiO_{1-x} plasma parameters with x of 0.3, 0.5, and 0.7 for the different laser energies reflecting various laser pulse intensities. The line intensity ratio method was used to get these values from the intensity ratio of two spectral lines obtained during the same ionization phase. All computed plasma parameters (λ_D , f_p , and N_D) satisfy the plasma definition criteria. When the laser energy increases, the values of λ_D and N_D decrease, and this change correlates with the changes observed in f_p and n_e . This is supported by Mohammed [23] and Hachim and Aadim [24].

Table 1: The ZnO_xNiO_{1-x} plasma parameters at x=0.3 in the air.

E (mJ)	T _e (eV)	n _e ×10 ¹⁸ (cm ⁻³)	f _p (Hz) ×10 ¹³	λ _D ×10 ⁻⁶ (cm)	N _d
700	0.446	12.182	3.134	1.421	147
800	0.451	13.644	3.317	1.350	141
900	0.468	14.131	3.376	1.352	146
1000	0.491	14.619	3.433	1.361	154

Table 2: The ZnO_xNiO_{1-x} plasma parameters at x=0.5 in the air.

E (mJ)	T _e (eV)	n _e ×10 ¹⁸ (cm ⁻³)	f _p (Hz) ×10 ¹³	λ _D ×10 ⁻⁶ (cm)	N _d
700	0.470	10.720	2.940	1.555	169
800	0.480	11.208	3.006	1.538	171
900	0.484	12.182	3.134	1.481	166
1000	0.486	14.131	3.376	1.377	155

Table 3: The ZnO_xNiO_{1-x} plasma parameters at x=0.7 in the air.

E (mJ)	T _e (eV)	n _e ×10 ¹⁸ (cm ⁻³)	f _p (Hz) ×10 ¹³	λ _D ×10 ⁻⁶ (cm)	N _d
700	0.474	12.182	3.134	1.466	161
800	0.486	13.157	3.257	1.427	160
900	0.488	14.131	3.376	1.381	156
1000	0.489	15.106	3.490	1.336	151

The electron temperatures were determined from the slope of the best linear fit in the Boltzmann plot, which requires peaks that originate from the same atomic species and the same ionization stage. Four peaks for ZnI species were chosen at 307.59, 330.25, 334.50 and 636.23 nm for ZnO_xNiO_{1-x} at x=0.3, 0.5, and 0.7 employing various laser energies, as shown in Figs. 4-6, where the energies of the levels, statistical weights, and transition probabilities used for the experimental plots of each element were obtained from the National Institute of Standard Technology database (NIST). The electron temperature is equal to the invert of the slope of the fitting line which equals to -1/k_BT. The fitting equations and the R² values are shown in the figure for all the fitting lines. R² is a statistical coefficient indicating the goodness of the linear fit, which takes a value between (0, 1).

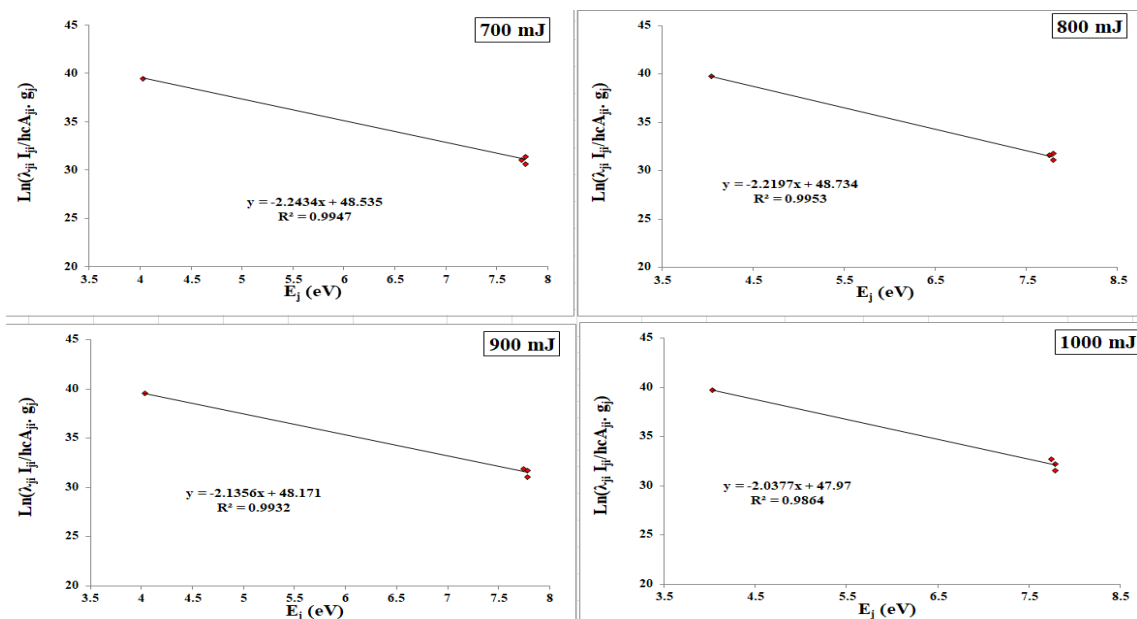


Figure 4: Boltzmann plots of plasma emission for ZnO_xNiO_{1-x} at x=0.3 for different laser energies.

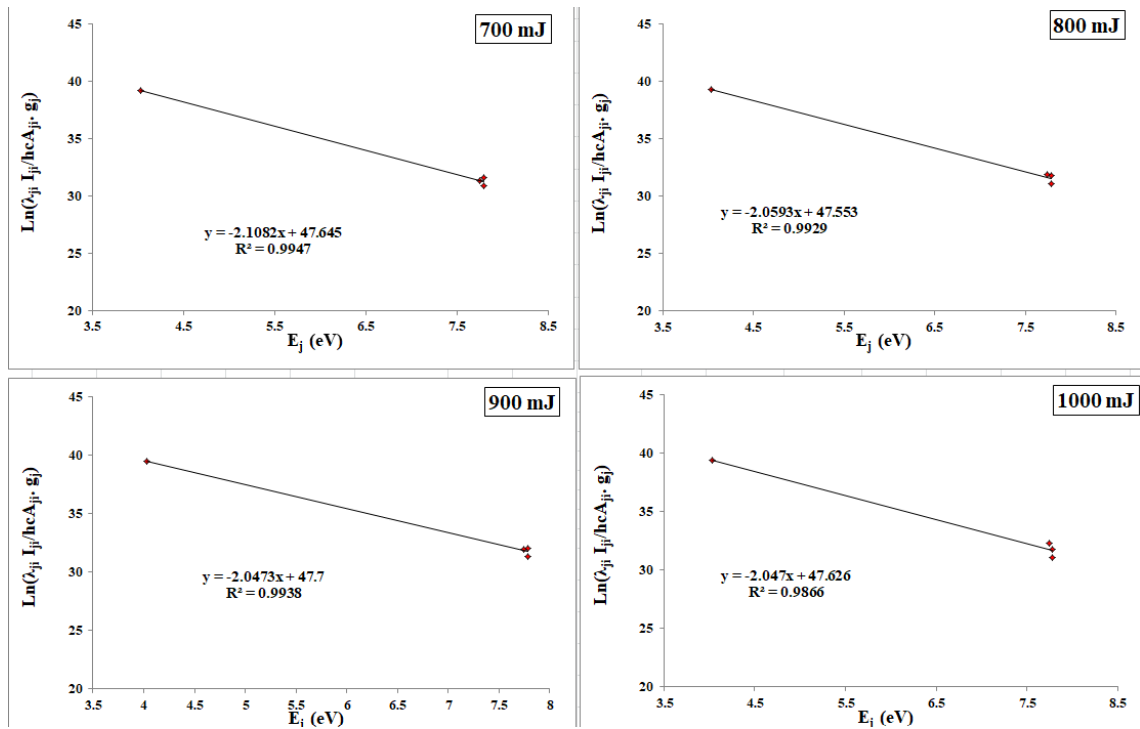


Figure 5: Boltzmann plots of plasma emission for ZnO_xNiO_{1-x} at x=0.5 for different laser energies.

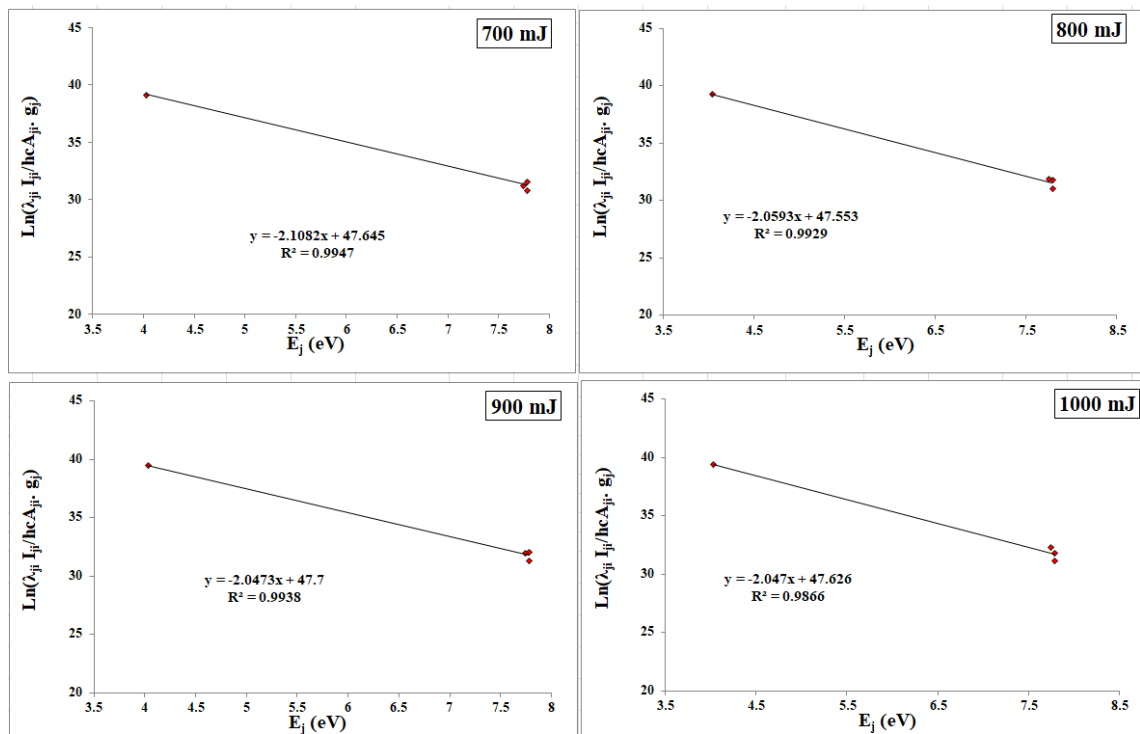


Figure 6: Boltzmann plots of plasma emission for ZnO_xNiO_{1-x} at x=0.7 for different laser energies.

Figs. 7-9 show the changes of T_e and n_e with laser energy using the line intensity ratio method for ZnO_xNiO_{1-x} at x=0.3, 0.5, and 0.7.

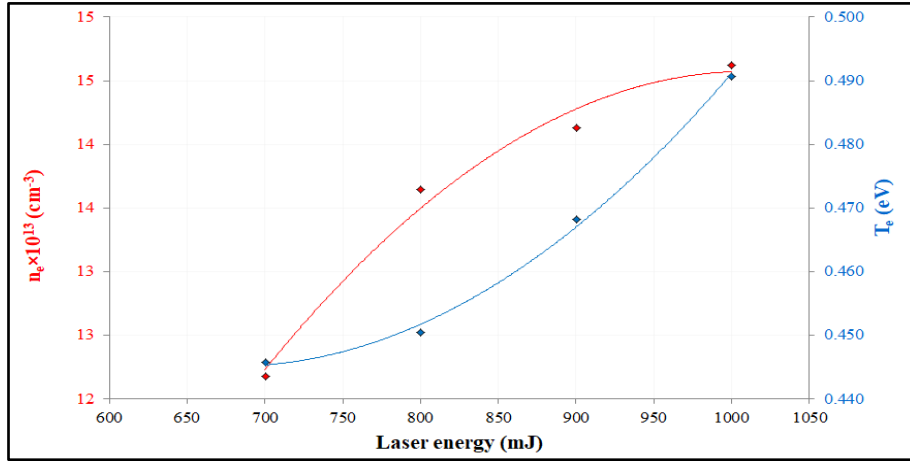


Figure 7: The changes of (T_e) and (n_e) with the laser energy for ZnO_xNiO_{1-x} at $x=0.3$ in the air.

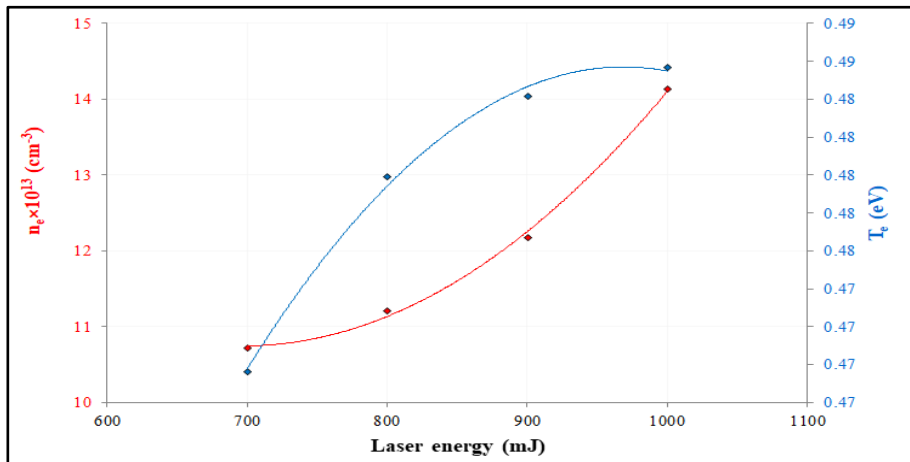


Figure 8: The changes of (T_e) and (n_e) with the laser energy for ZnO_xNiO_{1-x} at $x=0.5$ in the air.

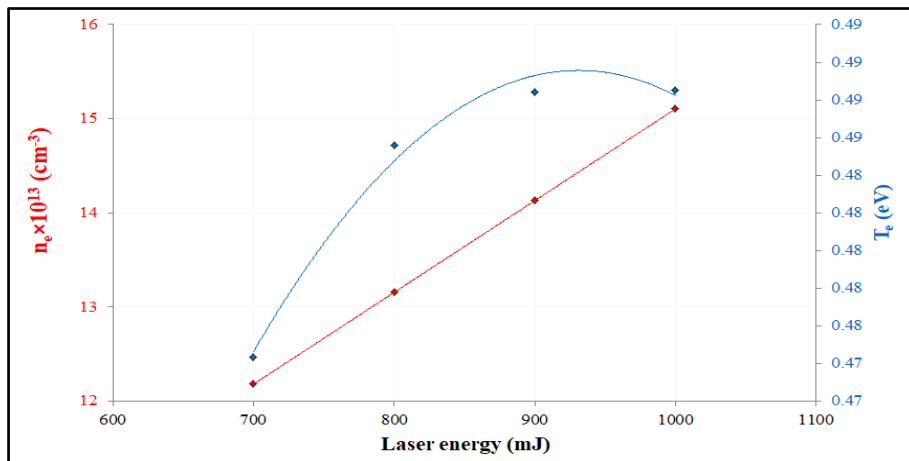


Figure 9: The changes of (T_e) and (n_e) with the laser energy for ZnO_xNiO_{1-x} at $x=0.7$ in the air.

The electron temperature values were obtained by evaluating the ratio of the intensities between two spectral lines linked to an atom or ion within the same radiation stage. T_e demonstrated an increase corresponding to the rise of the laser energy and electron density at a wavelength of 1064 nm across various laser peak powers.

4. Conclusions

A noticeable correlation was observed between the pulsed laser energy and the intensity of the spectral lines emitted from the laser-induced plasma, which increased with the increase in the laser energy. Under identical operational settings, the values of electron density (n_e) and plasma frequency (f_p) decreased in the case of LIBS in the air environment. Conversely, the values of electron temperature (T_e), Debye number (N_D), and Debye length (λ_D) exhibited an increase. Through these results, we obtain the best conditions for zinc oxide elements combined with nickel oxide in solar cell applications.

Acknowledgements

Funding for this research came from the University of Baghdad's Plasma Physics Lab. in the Physics Department of the College of Science.

Conflict of interest

Authors declare that they have no conflict of interest.

References

1. C. Pasquini, J. Cortez, L. M. C. Silva, and F. B. Gonzaga, *Journal of the Brazilian Chemical Society* **18**, 463 (2007). <https://doi.org/10.1590/S0103-50532007000300002>.
2. J. D. Pedarnig, S. Trautner, S. Grünberger, N. Giannakaris, S. Eschlböck-Fuchs, and J. Hofstadler, *Appl. Sci.* **11**, 9274 (2021). <https://doi.org/10.3390/app11199274>.
3. C. Fabre, *Spectrochim. Acta Part B Atom. Spect.* **166**, 105799 (2020). <https://doi.org/10.1016/j.sab.2020.105799>.
4. A. Botto, B. Campanella, S. Legnaioli, M. Lezzerini, G. Lorenzetti, S. Pagnotta, F. Poggialini, and V. Palleschi, *J. Analyt. Atom. Spectrom.* **34**, 81 (2019). <https://doi.org/10.1039/c8ja00319j>.
5. D. A. Gonçalves, G. S. Senesi, and G. Nicolodelli, *Tren. Envir. Analyt. Chem.* **30**, e00121 (2021). <https://doi.org/10.1016/j.teac.2021.e00121>.
6. A. Królicka, A. Maj, and G. Łój, *Materials* **16**, 6641 (2023). <https://doi.org/10.3390/ma16206641>.
7. S. Bashir, M. S. Rafique, C. S. Nathala, A. A. Ajami, W. Husinsky, and K. Whitmore, *J. Optic. Soci. America B* **37**, 2878 (2020). <https://doi.org/10.1364/josab.394695>.
8. R. Duclous, V. Tikhonchuk, L. Gremillet, B. Martinez, T. Leroy, P.-E. Masson Laborde, J.-C. Pain, and A. Decoster, *Phys. Plas.* **31**, 022904 (2024). <https://doi.org/10.1063/5.0162336>.
9. N. A. Shepelin, Z. P. Tehrani, N. Ohannessian, C. W. Schneider, D. Pergolesi, and T. Lippert, *Chem. Soci. Rev.* **52**, 2294 (2023). <https://doi.org/10.1039/D2CS00938B>.
10. S. A. K. Raheem, S. A. A.-H. Hatif, and A. H. Ali, *J. Univer. Babyl. Pure Appl. Sci.* **31**, 147 (2023). <https://doi.org/10.29196/jubpas.v31i3.4836>.
11. D. R. Bates and B. Bederson, *Advances in Atomic and Molecular Physics* (USA, Academic Press, 1985).
12. A. El Sherbini, T. M. El Sherbini, H. Hegazy, G. Cristoforetti, S. Legnaioli, V. Palleschi, L. Pardini, A. Salvetti, and E. Tognoni, *Spectrochim. Acta Part B Atom. Spectr.* **60**, 1573 (2005). <https://doi.org/10.1016/j.sab.2005.10.011>.
13. G. A. Alharshan, C. Eke, and M. Al-Buriah, *Rad. Phys. Chem.* **193**, 109938 (2022). <https://doi.org/10.1016/j.radphyschem.2021.109938>.
14. H. Amamou, A. Bois, B. Ferhat, R. Redon, B. Rossetto, and P. Matheron, *J. Quant. Spectr. Rad. Trans.* **75**, 747 (2002). [https://doi.org/10.1016/S0022-4073\(02\)00040-7](https://doi.org/10.1016/S0022-4073(02)00040-7).
15. M. P. Polek, M. C. Phillips, F. N. Beg, and S. S. Harilal, *AIP Advances* **14**, 025043 (2024). <https://doi.org/10.1063/5.0190522>.
16. K. A. Aadim, *Iraqi J. Phys.* **16**, 1 (2018). <https://doi.org/10.30723/ijp.v16i38.3>.
17. E. Gao, R. Wei, D. Zhang, Z. Zhu, Q. Gao, and B. Li, *J. Analyt. Atom. Spectr.* **38**, 1116 (2023). <https://doi.org/10.1039/d3ja00044c>.
18. T. Völker and I. B. Gornushkin, *J. Quant. Spectr. Rad. Trans.* **310**, 108741 (2023). <https://doi.org/10.1016/j.jqsrt.2023.108741>.
19. E. Alonso-Monsalve and D. I. Kaiser, *Phys. Rev. D* **108**, 125010 (2023). <https://doi.org/10.1103/PhysRevD.108.125010>.
20. N. K. Abdaalameer, S. Mazhir, and K. A. Aadim, *Chalcogen. Lett.* **18**, 405 (2021). <https://doi.org/10.15251/cl.2021.187.405>.
21. A. S. Wasfi, H. R. Humud, and M. E. Ismael, *Iraqi J. Phys.* **13**, 14 (2015). <https://doi.org/10.30723/ijp.v13i27.259>.

22. A. A. Abdullah, S. J. Mohammed, and G. H. Mohammed, Tikrit J. Pure Sci. **24**, 63 (2019).
<https://doi.org/10.25130/tjps.v24i2.354>.
23. R. S. Mohammed, K. A. Aadim, and K. A. Ahmed, Iraqi J. Sci. **63**, 3711 (2022).
<https://doi.org/10.24996/ijs.2022.63.9.5>.
24. H. S. Hachim and K. A. Aadim, Iraqi J. Sci. **63**, 5270 (2022).
<https://doi.org/10.24996/ijs.2022.63.12.16>.

الانبعاث الطيفي البصري لأوكسيد الزنك المشوب بأوكسيد النيكل لحساب معلمات البلازما باستخدام طريقة بولتزمان-بلوت

منى احمد عيسى¹ وكاظم عبد الواحد عادم¹
قسم الفيزياء، كلية العلوم، جامعة بغداد، بغداد، العراق

الخلاصة

استخدمت الدراسة طريقة التحليل الطيفي للإشعاع الضوئي لتقديم تأثير تغيير نسب الإضافة وطاقة الليزر على معلمات البلازما. تم الحصول على أطياف البلازما عبر طيف من مستويات الطاقة لاكسيد الزنك الممزوج بأوكسيد النيكل $ZnO_{(x)}NiO_{1-x}$ عند $x=0.3, 0.5, 0.7$. تم إجراء تحليل لهذه الخلائط المحمولة جواً من خلال تطبيق الطيفية. أشارت نتائج درجة حرارة الإلكترونات إلى أن النطاق بالنسبة لـ $x=0.3$ كان $0.446-0.491$ إلكترون فولت، ولـ $x=0.5$ كان $0.470-0.486$ إلكترون فولت، ولـ $x=0.7$ كان $0.474-0.489$ إلكترون فولت. يمكن أن تؤدي الفروقات في درجات حرارة الإلكترونات بين التراكيب إلى تطبيقات تكنولوجية جديدة وفهم الظواهر الفيزيائية. وُجد أنه عند زيادة نسبة الإضافة، تزداد شدة الخطوط الطيفية ودرجة حرارة الإلكترونات (T_e) وعدد ديباي (N_D) وطول دباي (λ_D)، في حين تنخفض كثافة الإلكترونات (n_e) وتردد البلازما (f_p) مع زيادة طاقة الليزر. وقد حدثت خطوط انبعاث المواد المخلوطة بشكل أكثر تكراراً في المادة المختلطة. من خلال هذه النتائج، نحصل على أفضل الظروف لتطبيقات خلايا الشمسية لعناصر أكسيد الزنك المدمجة مع أكسيد النيكل.

الكلمات المفتاحية: أكسيد الزنك (ZnO)، التحليل الطيفي للانبعاث البصري (OES)، بولتزمان-بلوت، أكسيد النيكل (NiO)، الاستئصال بالليزر.